nature materials

Review article

https://doi.org/10.1038/s41563-024-01962-5

Cavity-enhanced energy transport in molecular systems

Received: 14 July 2023

Accepted: 1 July 2024

Published online: 9 August 2024

Check for updates

Gal Sandik[1], Johannes Feist[2] ✉, Francisco J. García-Vidal[2] ✉ & Tal Schwartz[1] ✉

Molecules are the building blocks of all of nature's functional components, serving as the machinery that captures, stores and releases energy or converts it into useful work. However, molecules interact with each other over extremely short distances, which hinders the spread of energy across molecular systems. Conversely, photons are inert, but they are fast and can traverse large distances very efficiently. Using optical resonators, these distinct entities can be mixed with each other, opening a path to new architectures that benefit from both the active nature of molecules and the long-range transport obtained by the coupling with light. In this Review, we present the physics underlying the enhancement of energy transfer and energy transport in molecular systems, and highlight the experimental and theoretical advances in this field over the past decade. Finally, we identify several key questions and theoretical challenges that remain to be resolved via future research.

In nature, light and molecules are constantly interacting, with photons being absorbed or emitted, thereby driving a multitude of molecular events and photochemical reactions. These interactions, which normally occur in an irreversible manner and with a characteristic timescale of several femtoseconds, can change dramatically when they take place within photonic structures that act to confine the electromagnetic (EM) field. Under such confinement, the light–matter interaction strength can be enhanced to the point where it overcomes all of the dissipative, incoherent processes in the system, which fundamentally changes its nature.

Over the past decade, it has gradually been established that by 'dressing' molecules with the EM field in this regime of strong light–matter coupling, their properties can be modified, which offers new and exciting pathways for tailoring materials and controlling their chemistry[1,2]. One of the most dramatic manifestations of strong light–molecule coupling is its ability to mediate molecular interactions over macroscopic distances and enhance energy transport by several orders of magnitude. Molecular excitons are typically tightly bound, and therefore molecules can exchange energy via dipole–dipole (Förster-type) or electron-exchange (Dexter-type) interactions[3], which are inherently short-ranged. Moreover, molecular systems are often highly disordered. As a result, energy transfer (that is, the transmission of energy from one molecular species to another) and energy transport (exciton migration across a single-species molecular ensemble) are only efficient over nanometric length scales, with exciton migration occurring as a random hopping process between neighbouring molecules. However, this picture changes completely under strong coupling, where the entire molecular ensemble interacts simultaneously and coherently with the optical modes of the structure. Now, hybrid light–matter states, known as cavity polaritons, are formed as a mixture of the EM mode and the molecular excitations (see Box 1). Rather than being localized on individual molecules, the polaritonic wavefunctions are instead extended over a macroscopic number of molecules. The length scales of the polaritonic wavefunction are comparable to the optical wavelength, and may be even larger. As a result, the interactions between distant molecules obtain a non-local nature, which in turn facilitates the transfer of energy between them, as well as the transport of energy across macroscopic distances.

The first indication of this unusual state was the observation that spontaneous emission from molecules under strong coupling

[1]School of Chemistry, Raymond & Beverly Sackler Faculty of Exact Sciences and Center for Light–Matter Interaction, Tel Aviv University, Tel Aviv, Israel. [2]Departamento de Física Teórica de la Materia Condensada and Condensed Matter Physics Center (IFIMAC), Universidad Autónoma de Madrid, Madrid, Spain. ✉e-mail: johannes.feist@uam.es; fj.garcia@uam.es; talschwartz@tau.ac.il

https://doi.org/10.1038/s41563-024-01962-5

BOX 1

Strong coupling and polaritons

When a collection of N molecules, represented as two-level quantum emitters, is embedded inside an optical resonator, the system can be described by an extended coupled oscillator model, which is commonly used for understanding a wide collection of physical phenomena. Here one (quantum) oscillator represents an EM mode of the optical structure (for example, a standing-wave mode formed between the mirrors of a Fabry–Pérot cavity), which is coupled with the excitonic transitions in the N molecules. This system is described by the Hamiltonian

$$\hat{H} = \begin{pmatrix} E_{\mathrm{ph}} - \frac{i\hbar\kappa}{2} & g_1 & g_2 & \cdots & g_N \\ g_1 & E_{\mathrm{ex}}^{(1)} - \frac{i\hbar\gamma}{2} & & & \\ g_2 & & E_{\mathrm{ex}}^{(2)} - \frac{i\hbar\gamma}{2} & & \\ \vdots & & & \ddots & \\ g_N & & & & E_{\mathrm{ex}}^{(N)} - \frac{i\hbar\gamma}{2} \end{pmatrix} \quad (1)$$

where E_{ph} is the energy of the cavity mode, $E_{\mathrm{ex}}^{(i)}$ are the exciton energies, κ and γ are the decay rates of the cavity mode and the molecules, respectively, $\hbar$ is the reduced Planck constant and g_i represents the dipolar coupling strength, given roughly by $g \simeq d\sqrt{E_{\mathrm{ph}}/\epsilon V_{\mathrm{c}}}$. Here, d is the transition dipole element of the molecular transition, ϵ is the dielectric constant within the cavity and V_{c} is the effective cavity mode volume, which quantifies the spatial extent of the EM field. The simultaneous interaction of the EM mode with the entire molecular ensemble gives rise to collective coupling, which is quantified by the vacuum Rabi frequency $\Omega_{\mathrm{R}} = \frac{2}{\hbar} g\sqrt{N}$ (assuming identical molecules and identical coupling strengths, for simplicity)[63].

In the 'strong coupling' regime, defined by $\Omega_{\mathrm{R}} > \frac{1}{2}\sqrt{\kappa^2 + \gamma^2}$ (ref. 108), this Hamiltonian gives two distinct solutions, $|P^{(+)}\rangle$ and $|P^{(-)}\rangle$, which represent the new (upper and lower) polaritonic states of the system. These are hybrid excitations, which form as linear combinations of the cavity mode and the excitons. It is worth noting that, owing to the collective coupling, the Rabi frequency is proportional to the transition dipole element multiplied by the number density of molecules ρ, that is, $\Omega_{\mathrm{R}} \propto d\sqrt{N/V_{\mathrm{c}}} \propto d\sqrt{\rho}$. Typical molecular systems, with ~10^{10} molecules in a volume of ~λ^3 at optical frequencies (where λ denotes the wavelength), can thus reach particularly high coupling strengths of hundreds of millielectronvolts, and even up to 1.8 eV (ref. 109), facilitating the emergence of strong coupling conditions.

In addition to the polaritonic states, and in contrast to single-emitter strong coupling, the collective coupling also leads to the formation of $N-1$ dark states with an energy E_{ex}, which also exhibit collective behaviour to some extent[110,111]. In reality, this rather simple picture is further complicated due to energetic disorder in the molecules, non-identical coupling resulting from the field inhomogeneity within the cavity or random molecular orientations, and other effects that are not accounted for by this basic Hamiltonian.

Dispersion relation and group velocity

In many types of optical structure, specifically those which possess some translational symmetry, the energy of the EM resonance is not fixed but rather changes continuously, forming a band (or several bands) of photonic modes. For example, in the planar cavity depicted in panel **a**, the mode energy depends on the in-plane component of the wave vector $k_{\parallel}$. For light confined between the mirrors, constructive interference among the multiple reflections leads to the creation of standing-wave modes, similar to standing waves on a string or a quantum particle in a box. Imposing the appropriate boundary conditions at the mirrors yields the dispersion relation for photons trapped within the cavity, which, in its simplest form, is

$$E_{\mathrm{ph}}^{(m)}(k_{\parallel}) = E_m\sqrt{1 + \left(\frac{k_{\parallel} n L_{\mathrm{cav}}}{\pi m}\right)^2}. \quad (2)$$

Here L_{cav} is the distance between the mirrors, $n = \sqrt{\epsilon}$ is the background refractive index inside the cavity, m is an integer signifying the mode order and $E_m = \frac{hcm}{2L_{\mathrm{cav}}n}$ is the normal-incidence (that is, $k_{\parallel}=0$) resonance energy where c is the speed of light and h is the Planck constant. As illustrated in panel **b**, under strong coupling this dispersion curve splits around the crossing point with E_{ex} to form two dispersive polaritonic branches, separated by $\hbar\Omega_{\mathrm{R}}$. At that resonance point, the polaritons are an equally weighted superposition of light and matter. However, owing to the cavity dispersion, and as shown in

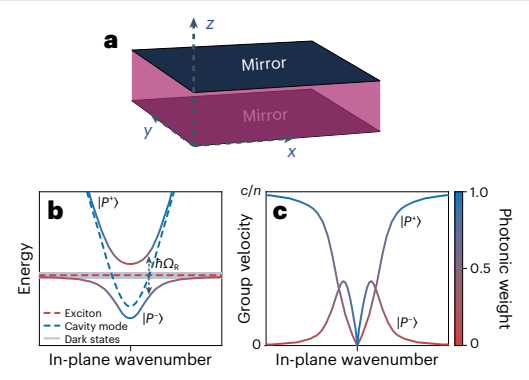

Fundamentals of cavity polaritons. a, Fabry–Pérot cavity, which comprises two planar mirrors (for example, metal films) and a dielectric layer, embedded with dye molecules, between them. The EM mode is confined in the vertical direction but propagates parallel to the mirrors, with an in-plane wavenumber $k_{\parallel}$. **b**, Dispersion curves for the cavity photons (dashed blue line) and for the upper $|P^{(+)}\rangle$ and lower $|P^{(-)}\rangle$ polaritons (solid lines) formed under strong coupling. The red dashed line marks the bare-exciton energy E_{ex} and the grey shaded area represents the $N-1$ dark states. The graduated line colouring indicates the variation in the photonic weight $\overline{W}_{\mathrm{ph}}$ across the polariton branches. **c**, Polariton group velocities extracted from the polariton dispersion curves. Note that at high $k_{\parallel}$ values, where the lower polariton energy converges to E_{ex}, its group velocity tends to zero, which is characteristic of the uncoupled exciton. Conversely, the upper polariton asymptotically reaches the speed of light in the dielectric medium as its energy shifts further away from the exciton. This behaviour is in line with the variation of photonic weight across the polariton branches, which reaches a value of zero or unity for the lower and upper branches, respectively.

(continued from previous page)
b, this composition varies across the polariton branches, with the photonic weight of the upper (+) and lower (−) polaritons given by

$$\overline{W}_{\mathrm{ph}}^{\pm} = \frac{1}{2}\left(1 \mp \frac{\Delta^2}{(\hbar\Omega_{\mathrm{R}})^2 + \Delta^2}\right), \quad (3)$$

where $\Delta = E_{\mathrm{ex}} - E_{\mathrm{ph}}$ and the excitonic weight being $\overline{W}_{\mathrm{ex}} = 1 - \overline{W}_{\mathrm{ph}}$.

The polariton dispersion can be measured spectroscopically, in a similar manner to bare molecular transitions. However, in addition to the requirement for energy matching between the incoming photons and the energy of the transition, it is also required that the in-plane wavenumber of the photons (which is related to the wavelength λ and the incident angle θ by $k = 2\pi/\lambda \times \sin\theta$) is exactly matched with that of the particular polaritonic state being probed. Alternatively, once excited, polaritons may decay radiatively, by emitting a photon from the cavity at an angle dictated by the same in-plane wavenumber conservation, together with the cavity dispersion relation. From the polariton dispersion, their group velocity v_{g} (shown in panel **c**) can be deduced as $v_{\mathrm{g}} = \frac{1}{\hbar}\frac{\partial E^{(\pm)}}{\partial k_{\parallel}}$. Assuming that the bare excitons are immobile, it can be shown (see the Supplementary Information in ref. 21) that the polariton group velocity is directly related to its photonic weight and the photon group velocity, such that $v_{\mathrm{g}} = \overline{W}_{\mathrm{ph}}^{\pm}\left(\frac{1}{\hbar}\frac{\partial E_{\mathrm{ph}}}{\partial k_{\parallel}}\right)$, which can be viewed as a special case of the Hellmann–Feynman theorem. These relations express the fact that polaritons can indeed propagate, as opposed to the original localized molecular excitons, and that this propagation is a manifestation of their partially photonic character.

conditions exhibits long-range spatial coherence, which can extend over several micrometres[4]. This extraordinary result provided a clear signature of the extended nature of the polaritonic wavefunctions, and was also confirmed in a later study[5]. Soon thereafter, several pioneering publications reported, both experimentally and via numerical simulations, clear demonstrations of enhanced energy transport[6–10]. Notably, the collective, delocalized nature of polaritons was also shown to fundamentally alter intermolecular energy transfer between donor and acceptor molecules in a cavity[11,12], enabling its occurrence over distances exceeding 100 nm, far greater than the typical Förster distance[13]. These early studies demonstrated the technological potential of strong coupling and cavity-enhanced transport, specifically for the field of organic electronics, where the inefficient transport of excitons and charge carriers places severe constraints on device performance[14,15]. Furthermore, the possibility of combining the active nature of excitonic materials with this enhanced transport opens up new opportunities for ultrafast signal processing, all-optical control[16] and photonic architectures where organic materials are hybridized with inorganic semiconductors[17,18]. Over the past decade, the exciting opportunities offered by cavity-enhanced energy transport have driven the growing interest in this topic, which has led to substantial experimental and theoretical progress. Ultrafast optical techniques have been used to visualize directly the long-range motion of polaritons in strongly coupled molecular systems[10,19–23], as well as the time-resolved dynamics of intermolecular energy transfer[12,13,24–26]. In parallel, realistic models that take into account the molecular complexity and the various possible processes have been developed, aiming to capture the intricacies of this fascinating phenomenon[27–37]. In contrast to inorganic systems, organic molecules typically have a complex internal structure with vibronic (both vibrational and electronic) states and transitions, which can play a central role in the energy-transport process[38] and offer additional degrees of freedom for potentially controlling and making use of the transport properties. These features give molecules a unique role in that they could serve as both the active material and the photonic platform, enabling enhanced transport and redistribution of energy within a device. One example of such effects is seen in the condensation of polaritons as they thermalize while propagating along a plasmonic lattice[39,40]. Molecular systems under ambient conditions are inherently disordered, they are efficiently coupled with a surrounding thermal bath, and decay channels via transitions between the polaritonic states and other, non-coupled molecular energy levels, may also exist. Altogether, such effects lead to considerable deviations from a simple picture of ideal, plane-wave excitations spreading freely across the systems, which is often successfully used to describe transport in inorganic polaritonic systems[41–43]. Instead, recent time-resolved measurements[21] and advanced numerical simulations[32] have shown that energy transport in molecular strongly coupled systems is characterized by an interplay between ballistic and diffusive processes that result from two counteracting effects, namely random scattering due to molecular disorder and thermal fluctuations, and delocalization that stems from the photonic component.

With the hand-in-hand progress of theoretical modelling and experimental explorations, the inner workings of cavity-enhanced transport are gradually being disclosed. At the same time, these recent studies have clearly established that the underlying mechanisms that govern this phenomenon remain far from being fully understood, with every step in this research revealing new questions. This Review aims to present an up-to-date overview of cavity-enhanced energy transport, focusing on its recent exploration and implications in organic strongly coupled systems. In particular, we discuss the basic concepts of polaritonics in various architectures, the gradual development of theoretical modelling approaches and experimental studies of these systems, and the current understanding of the processes involved in cavity-enhanced energy transport. Finally, we address the potential implications of cavity-enhanced transport and the key challenges that are yet to be overcome to harness this fascinating phenomenon.

Photonic platforms for enhanced transport

The resonant optical confinement required for strong coupling can be achieved using numerous types of photonic structure that rely on different mechanisms. The modes of these structures can have very different spatial distributions, lifetimes and characteristic dispersions, which in turn affect the polaritons and the mechanism of enhanced energy transport. This section provides a brief survey of common photonic platforms used for cavity-enhanced transport—which are presented in Fig. 1—along with their properties and the main differences between them.

Planar microcavities

Perhaps the simplest optical resonator is a planar Fabry–Pérot microcavity, which is composed of two parallel mirrors, separated by a distance L_{cav}, such that a standing-wave mode can form between them (Fig. 1a). Metallic mirrors (for example, silver or gold) typically provide broadband reflectivity of up to 98% in the visible and infrared regions, with quality (Q) factors of 20–100 (or a lifetime of ~25 fs for visible light). Alternatively, distributed Bragg reflectors (DBRs) composed of low-loss dielectric layers give a much higher reflection, leading to Q factors of the order of 1,000 or more. However, this comes at the cost of a narrower reflection bandwidth and higher fabrication complexity. Moreover, in such dielectric cavities, the penetration depth of the field into the reflectors is of the order of several wavelengths. This penetration depth is much smaller in metals (of the order of 10 nm), which reduces the mode volume and increases the coupling strength[44]. The molecules are often uniformly distributed within the cavity, such that

https://doi.org/10.1038/s41563-024-01962-5

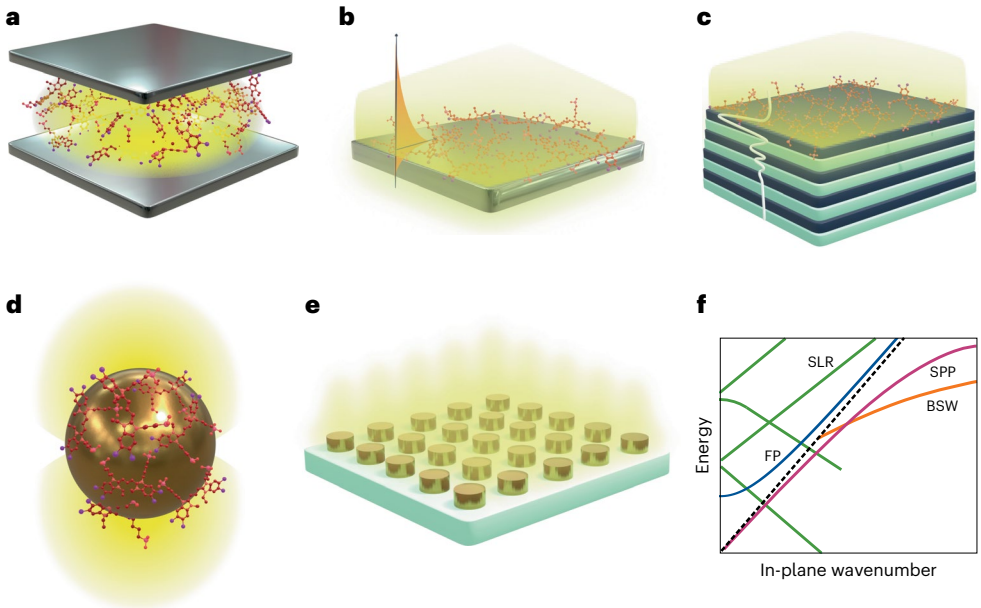

Fig. 1 | Prototypical geometries used for cavity-enhanced energy transport. **a**, A planar Fabry–Pérot cavity that consists of two mirrors and molecules between them interacting with the EM mode, which is formed as a standing wave in the direction perpendicular to the mirrors. **b**, A surface plasmon mode formed at the interface between a smooth metal film and air, with its magnitude decaying exponentially with the distance from the interface. **c**, Bloch surface wave, confined to the interface between a dielectric DBR structure and air. **d**, A gold nanoparticle with its localized plasmon mode interacting with molecules adsorbed on the nanoparticle surface. **e**, A periodic array of metallic nanodisks, where the localized plasmons interact to form a collective surface lattice resonance mode. **f**, Representative dispersion curves of the various photonic platforms: planar Fabry–Pérot (FP), surface plasmon polariton (SPP) on a metal film, Bloch surface wave (BSW) and surface lattice resonance (SLR). The dashed black line represents the air light line. Note that, unlike other types of mode, the Fabry–Pérot dispersion shows a minimum at $k_{\parallel} = 0$. Similarly, the BSW mode has a cut-off energy at the point where its dispersion reaches the light line[52] (where the mode is no longer confined), in a similar manner to the guided modes of a slab waveguide.

the molecules interact differently with the cavity mode, depending on the strength of the local electric field[45,46]. Therefore, the collective coupling (and overall energy splitting) incorporates all of the individual interactions within the cavity. However, the planar geometry readily lends itself to the fabrication of more elaborate multilayer structures. This enables the accurate positioning of the molecular layers at specific heights within the cavity, and a detailed examination of the (out-of-plane) energy transfer as the distance between the donor and acceptor layers is varied[13,47,48]. Finally, it should be noted that, unlike other geometries discussed below, the Fabry–Pérot dispersion has a minimum and, hence, the lower polariton has a vanishing group velocity at $k_{\parallel} = 0$ (see Box 1).

Electromagnetic surface waves

Confinement of light into a two-dimensional space can also be obtained in the form of EM surface waves. These are dispersive modes that are bound to the interface between two different media, exhibiting evanescent decay of the field away from that interface and propagating parallel to it. A well-known example is given by surface plasmon polaritons (SPPs)[49], which are transverse-magnetic-polarized waves formed at the boundary between a metal film and a dielectric material (or air) as a hybridization between light and charge oscillations in the metal (plasmons), as shown in Fig. 1b. When a molecular film is deposited on top of the metal surface, optimally located at the mode maximum, strong coupling between the SPPs and the molecular excitons can occur, forming surface plasmon–exciton–polaritons[50,51]. The in-plane wavenumber of SPPs is larger than the free-space wavenumber (for the same energy), which decouples them from free-space waves and gives them their surface-bound nature. In other words, their dispersion resides beyond the light line (Fig. 1f), and, therefore, to excite and probe the emerging exciton–polaritons, the wavenumber mismatch must be compensated using either prism coupling or grating coupling. SPPs, like other types of surface wave, can exhibit a steep dispersion, leading to large plasmon–exciton–polariton group velocities that are comparable to the speed of light. However, the large ohmic losses that are typical of metals result in short lifetimes, limiting the propagation to several micrometres. Another type of EM surface wave that can also lead to the formation of exciton–polaritons is Bloch surface waves (BSWs)[52,53] (Fig. 1c). As the optical analogue of the electronic surface states found at the edges of crystals, BSWs can form at the interface between a DBR and air (or other homogeneous dielectric medium). As with SPPs, the dispersion of BSW polaritons resides beyond the light line, but also within the bandgap of the DBR (a one-dimensional photonic crystal). This results in a mode profile that decays exponentially on both sides of the interface. The main advantage of BSWs over SPPs is their ultralow absorption loss, which results from the purely dielectric nature of the structure. This, together with their high group velocity, makes this system an ideal platform for enhanced energy transport. Similar advantages are also offered by dielectric nanowires[54].

Plasmonic nanoparticles and nanoparticle arrays

Metallic nanoparticles can exhibit a resonant optical response, which is sensitive to the size and geometry of the particle[49]. These resonances correspond to the excitation of 'localized surface plasmon' (LSP) modes, which can be coupled with the excitonic transition in molecules adsorbed on the particle surface[55,56]. Like SPPs in metal films, LSPs are also associated with a confined EM field (Fig. 1d); however, the confinement here occurs in three dimensions and over nanometric dimensions. On the one hand, LSPs have rather low Q factors of 1–10. On the other hand, this subwavelength mode volume enables strong coupling to be obtained with a much smaller number of molecules, down to the single-molecule scale for cases of extreme confinement[57,58]. Another fundamental difference with respect to the macroscopic geometries is that the LSPs form a discrete set of (non-dispersive) modes. These

features are particularly advantageous in numerical simulations of cavity-enhanced energy transfer, simplifying the microscopic treatment of both the molecular ensemble and the EM field.

When plasmonic nanoparticles are arranged in a periodic lattice with a spacing that is comparable to the optical wavelength, their individual modes can interact to form collective, delocalized modes, known as surface lattice resonances (SLRs)[59] (Fig. 1e). The discrete translational symmetry gives rise to a complex dispersion band structure, which can be tailored via the shape/size of the particles, the periodicity and the unit cell geometry. This flexibility makes SLRs highly attractive for cavity-enhanced energy transport, providing unique controllability over the transport properties of polaritons[32,60,61]. Moreover, both radiative and non-radiative losses can be suppressed for SLR modes despite residing within the light line, leading to much longer lifetimes, which benefits the enhancement of energy transport. SLRs can similarly form in arrays of dielectric particles[62], which exhibit even higher Q factors.

Theoretical approaches and modelling

The objective of this section is to briefly introduce the theoretical approaches that have been used to study cavity-modified energy transport in recent years. As most of the main concepts in the present section are well known in quantum optics and/or molecular physics, we forgo a mathematical analysis in favour of a schematic presentation of the key points of the different models.

The modelling of cavity-modified energy transport usually relies on a description of the interaction between the excitons of a collection of molecules and the quantized EM fields that are supported by the optical cavity. In the simplest approach, and following standard techniques used in quantum optics, the first models treated molecules as two-level systems, which accounts for the electronic transition between molecular ground and excited states, and the optical cavity is assumed to support a single EM mode[6–8,28]. The coupling strength between light and matter constituents, usually treated within the so-called dipolar and rotating-wave approximations, is proportional to both the transition dipole moments of the molecular excitons and the quantized electric field associated with the cavity mode. The resulting Hamiltonian is usually referred to as the Tavis–Cummings model[63]. Dispersion of the cavity mode with in-plane momentum, as present in Fabry–Pérot cavities or planar plasmonic structures, can also be incorporated into the framework[37,64–66]. To quantify the effect of the cavity on energy transport, bare intermolecular interactions need to be included in the Tavis–Cummings Hamiltonian. In addition to the coherent dynamics described by the Hamiltonian, different dissipative mechanisms are also present in the system, such as radiative and non-radiative losses associated with the molecules and cavity losses. The dynamics of the system can then be described through the master equation formalism developed for open quantum systems in which dissipative mechanisms are modelled using Lindblad terms, which describe frequency-independent dissipation rates[67]. In addition, to consider the initial excitation that triggers the exciton transport/transfer, a term that represents either coherent or incoherent pumping of the cavity or molecules must be introduced. Apart from its fundamental value, the simple modelling of the process described above has been used to study the effect of both spatial disorder and inhomogeneous broadening on the energy-transport characteristics, as these are inherent to organic molecules at room temperature[68].

Molecular energy transfer in the absence of a cavity has also been studied intensively in recent years, mainly in connection with light-harvesting processes[38,69,70]. By analysing energy transfer in these systems, it was realized that dissipation experienced by molecular excitations due to their internal vibronic structure is of paramount importance when dealing with energy transport in organic materials. To address these processes theoretically, researchers have developed several models and techniques, which have recently been adapted for the theoretical study of cavity-modified energy transport. Along this line, using a general Bloch–Redfield approach, the frequency-dependent spectral densities that characterize the local vibrational reservoir of each molecule have been used to account for the exciton–vibration coupling[27,29]. This Bloch–Redfield formalism treats the vibrational modes as a weakly coupled thermal bath and, therefore, does not account for the possible coherent exchange of energy between electronic and vibrational degrees of freedom within the molecules. Going beyond the Bloch–Redfield approach to fully capture the coupling between excitons and vibrational modes is an extremely challenging problem, due to the high number of vibrational degrees of freedom. So far, such studies have included only the interaction between a small ensemble of molecules and a single cavity mode, which has been analysed using advanced tensor network simulations[71], in which the vibrational modes are further restricted to be harmonic oscillators. An alternative way to fully incorporate the coupling between electronic excitations and vibrational degrees of freedom into the modelling is to use atomistic models to describe the internal structure of the molecules[30,32,72]. Using a hybrid quantum mechanics/molecular mechanics (QM/MM) framework, it has become feasible to simulate the interaction between thousands of organic molecules with a Fabry–Pérot cavity mode[32]. There, the electron–electron interaction was modelled at the Hartree–Fock level for the ground state and at the level of configuration interaction singles for the excited states. Similar approaches have also been used for treating phonons in polaritonic systems based on halide perovskites[22]. Finally, several promising methods that were recently developed could enable the simulation of systems containing large numbers of molecules at a reasonable cost, while still accounting for the complex vibrational structure of the molecules[73,74] (although these methods have not yet been applied to energy transport).

Cavity-enhanced intermolecular energy transfer

Intermolecular energy transfer occurs when an electronic excitation stored in a molecule (the donor) is transferred to another molecule (the acceptor) during the lifetime of the excited state. Generally, various mechanisms may dominate this hopping process, depending on the distance, electronic spin or strength of the interaction[3,75]. For example, Förster resonance energy transfer (FRET) results from a (perturbative) near-field dipole–dipole interaction, which decreases with the sixth power of the separation between molecules, with an effective interaction distance of the order of 5–10 nm and a rate constant determined by the spectral overlap between the donor emission and acceptor absorption spectra[76]. At very short distances, this interaction is strong enough to mix electronic states and the FRET process converts to the Redfield mechanism[29,77]. Dexter energy transfer is the exchange of two electrons between nearest neighbours and requires wavefunction overlap between donor and acceptor molecules, such that its rate decreases exponentially with distance and its effective range is around 1 nm. Therefore, the dominant process when molecules are separated by distances of a few nanometres is FRET. At the end of the last century, accompanying the emergence of nanophotonics, much attention was drawn to the effect that a complex photonic environment may have on this mechanism. Theoretical work from as early as the 1980s pointed out that the resonant dipole–dipole interaction is altered when mediated by a resonant mode in nanoparticles[78], cavities[79,80] and periodic structures[81,82]. In this century, it has been demonstrated that the range over which energy transfer occurs could be extended by coupling the molecules to a surface plasmon mode supported by a metal film, when operating in the weak light–matter coupling regime[83,84].

Energy transfer between two different molecular species placed in a microcavity and in the strong coupling regime was first reported in 2014[11], utilizing a blend of two types of cyanine dye placed together in a matrix between two metallic mirrors (Fig. 2a). Subsequently, the change in the donor lifetime in the presence of the acceptor was analysed[12], showing that the energy transfer rate was increased by a factor of seven under strong coupling conditions (when compared with

https://doi.org/10.1038/s41563-024-01962-5

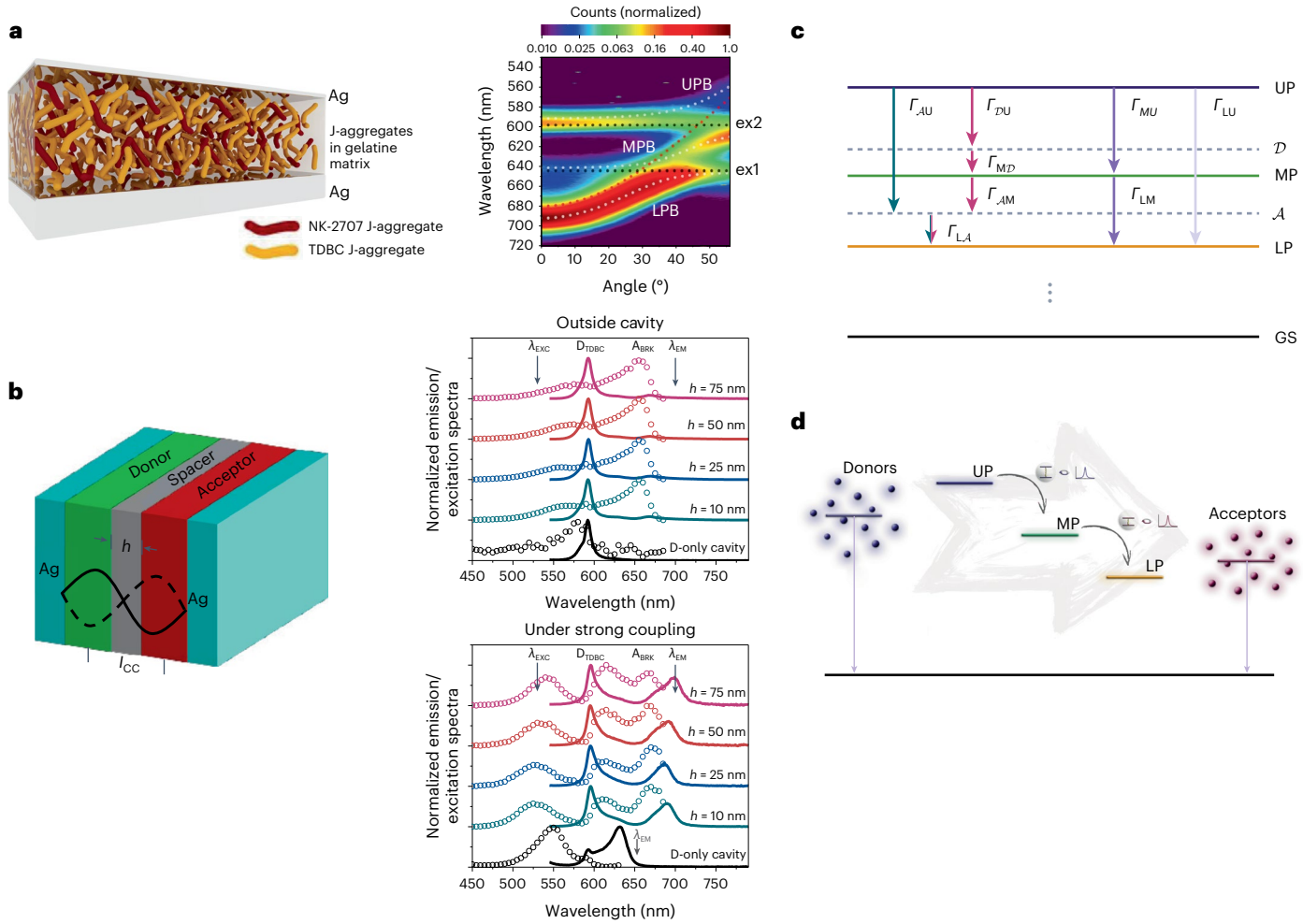

Fig. 2 | Cavity-mediated energy transfer. a, Left: the microcavity structure, as reported in ref. 11, comprises a 620-nm-thick layer of a blend of two different J-aggregates in a supporting matrix between two metallic mirrors. Right: the corresponding angle-dependent microcavity emission following excitation at 473 nm. UPB, upper polariton band; MPB, middle polariton band; LPB, lower polariton band; ex1, NK-2707 exciton energy; ex2, TDBC exciton energy. **b**, Left: schematic picture of the strongly coupled Fabry–Pérot cavity as studied in ref. 13. *h*, spacer thickness; l_{CC}, centre-to-centre distance between donor and acceptor layers. The black solid and dashed lines illustrate the field distribution of the cavity mode. Right: normalized excitation (open circles) and emission (solid line) in the absence of the top mirror (top) and in the closed cavity (bottom). λ_{EXC}, excitation wavelength; λ_{EM}, emission wavelength; D_{TDBC}, donor (TDBC dye); A_{BRK}, acceptor (BRK dye). **c**, Level scheme of the polaritons (as well as the two sets of dark states $\mathcal{D}$ and $\mathcal{A}$) showing various paths of decay, which are labelled with their corresponding rates Γ, as described in ref. 27. UP, upper polariton; MP, middle polariton; LP, lower polariton; GS, ground state. **d**, Schematic diagram of the mechanism of cavity-mediated energy transfer: excitation from the UP is funnelled to lower polaritons (MP and LP) and the two sets of dark states ($\mathcal{D}$ and $\mathcal{A}$, shown in **c**) using the local vibrational modes of the molecules as efficient channel reservoirs for decay[107]. Panels reproduced with permission from: **a**, ref. 11, Springer Nature Ltd; **b**, ref. 13, John Wiley and Sons; **c**, ref. 27, APS; **d**, ref. 107, Universidad Autónoma de Madrid.

the rate outside the cavity). Shortly afterwards, this energy-transfer mechanism was reproduced for a study in which the two organic species were physically separated inside the cavity[13]. In this case, we can refer properly to long-range energy transfer, as the excitation, when placed in the donor molecules, is then transferred to the acceptors that are located more than one hundred nanometres away (Fig. 2b). A transfer efficiency of about 37% was estimated, and the energy-transfer process was shown to be independent of the distance between the donor and acceptor molecules for a given coupling strength. This capability was subsequently corroborated, and its range increased using thin films of two J-aggregated molecular dyes immersed in a microcavity and separated by a spacer layer with a thickness of 2 µm (ref. 47). As shown below, energy transfer is also very sensitive to the energy landscape. It has been reported that the long-range energy-transfer efficiency can also be enhanced by tuning the frequency of the cavity mode in negatively detuned cavities[85].

At the time that it was first reported in 2017, although it was acknowledged that the delocalized character of the formed polaritons played a key role[8], the underlying physical mechanism responsible for the long-range energy transfer was not well understood. Since then, several theoretical groups have applied different models to gain a fundamental picture of this process. What we describe in this Review is the basic consensus of all of these theoretical approaches[27–29]. Before analysing the mechanism for long-range energy transfer, it is worthwhile to first examine the energy-level structure associated with the system, that is, a macroscopic collection of two types of molecule interacting with a cavity mode. As discussed in Box 1, for an ensemble of identical molecules strongly coupled to a cavity mode, two delocalized polaritons emerge: the lower polariton and the upper polariton, whose energies are separated by the so-called Rabi splitting $\hbar\Omega_R$. In addition, a set of (degenerate) dark states, which are superpositions of molecular excited states that do not couple to the cavity mode, appear. If the cavity hosts two types of molecule (both of which are strongly coupled), apart from the upper polariton and the lower polariton, a third polariton arises, the middle polariton. In addition, there are two collections of dark states, each associated with one type of molecule

https://doi.org/10.1038/s41563-024-01962-5

and thus degenerate at the corresponding energies. As mentioned above, polaritons are hybrid states, partly light and partly matter. The upper polariton branch mainly results from the hybridization of the cavity mode and donor molecules, whereas the lower polariton branch is composed mainly of acceptor states mixed with the optical field. Finally, the middle polariton branch contains a mixture of states in which both types of molecule have similar weights. To trigger the energy-transfer process, the donor molecules need to be excited by pumping the cavity at the upper polariton frequency. By looking at the population of the lower polariton, which is composed mostly of acceptor states, we can quantify the transfer efficiency. All of the possible channels that lead the population from the upper polariton to the lower polariton are shown in Fig. 2c. Numerical results based on a Bloch–Redfield approximation to perturbatively consider vibrational modes in the Tavis–Cummings Hamiltonian[27], as described above, show that the main pathway that leads to energy transfer from donor to acceptor molecules corresponds to the red route. The population is carried from the upper polariton to the lower polariton through the middle polariton and the two sets of dark states due to local exciton–vibration interactions[86], as depicted schematically in Fig. 2d. The mixed composition of the middle polariton, which combines donor and acceptor molecule populations in similar proportions, is crucial for this boost in energy transfer. Importantly, this general picture applies not only to the case in which donor and acceptor molecules are intermixed but also when the two types of molecule are spatially separated[13,48], in accordance with the experimental findings, where the Rabi splitting is the key parameter in this energy-transfer process. Very recently, it has also been demonstrated that intermolecular couplings, which were not included in the modelling, can modify this picture by creating bands of polariton states such that energy can cascade more efficiently through these states from the upper polariton to the lower polariton[26]. For molecules where the vibrations cannot be described perturbatively (which applies to most non-aggregated fluorescent dyes), the alternative simple picture of radiative pumping usually describes experiments well[11,87], even if a rigorous derivation from a first-principles Hamiltonian is not available. Here, the coupling from the dark-state reservoirs to the polaritons is assumed to be determined by the spectral overlap between the bare-molecule emission spectrum and the polariton absorption spectrum, in direct analogy to the same quantity appearing in FRET[76]. Inspired by the work on exciton long-range energy transfer, a recent experimental study has demonstrated that it is also feasible to transport vibrational energy by strongly coupling the relevant vibrational modes of the molecules with the cavity modes supported by an infrared cavity[24].

Enhanced transport in organic semiconductors

The polaritonic states, as previously mentioned, are collective delocalized states. As such, different molecules no longer behave as individual entities but rather as correlated objects, which had already been recognized in early theoretical studies[64,88]. This concept was then demonstrated in a pioneering experiment[4] in which molecules under strong coupling to surface plasmons were shown to emit coherently with each other, producing a clear interference pattern up to intermolecular distances of several micrometres (see Fig. 3a,b). Such long-range coherence necessitated that phase information was communicated between distant molecules, and, therefore, it pointed towards enhanced transport over distances that are far beyond the molecular scale. Moreover, numerical simulations have shown that exciton conductance across a disordered chain of two-level molecules, which normally decays exponentially with the system size, can be enhanced by many orders of magnitude via strong coupling to a cavity mode[6,7].

The first experimental demonstration of such enhanced exciton transport was realized using BSW polaritons, benefiting from the ultralong propagation distances enabled by their low-loss nature and the high v_g associated with BSWs. Using steady-state emission

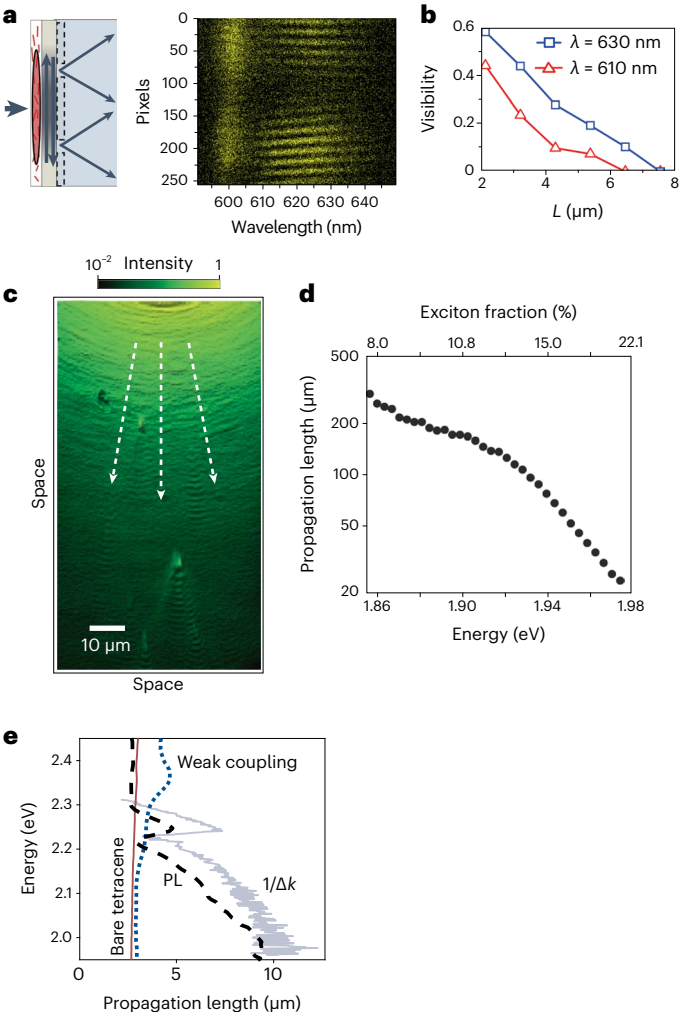

Fig. 3 | Steady-state measurements of long-range coherence and the long-range transport of polaritons. a, Right: interference fringes resulting from overlapping of the spontaneous emission collected from two different locations on a molecular film under strong coupling with surface plasmons, marking the long-range spatial coherence under strong coupling[4]. Left: sketch illustrating the light emitted from the sample (under wide-field non-resonant excitation), which is then collected and overlapped at the plane of the sensor. The interference fringes appear only at the wavelength range of 610–640 nm, corresponding to the lower-branch polaritons, whereas uncoupled emission (around 600 nm) does not produce any fringes. The appearance of interference fringes within the emission of spatially separated polaritons signifies the long-range phase coherence of polaritons, which further demonstrates the delocalized nature of the polaritonic wavefunctions. Close to 600 nm (the bare-exciton wavelength) no interference fringes appear, as expected for the spatially incoherent emission from independent point sources. **b**, Fringe visibility as a function of the distance L between the two points from which the polariton emission was collected, demonstrating the micrometre-scale coherence length for polaritonic emission. **c**, Real-space image of BSW polariton emission, under focused steady-state excitation (at the top edge of the image)[9]. The emission emanating from points located more than 100 μm away from the excitation spot provides direct visualization of the long-range transport of polaritons. **d**, Propagation length, extracted from the emission pattern in **c**, as a function of the polariton energy/excitonic weight. **e**, Comparison between the inverse width of the polariton dispersion ($1/\Delta k$, grey) and the propagation length of polaritons (under strong coupling with SLR modes, black dashed line) extracted from real-space emission patterns, at different polariton energies[61]. The red line marks the measured propagation length for bare excitons and the blue dotted line corresponds to the case of weak coupling. PL, photoluminescence. Panels reproduced with permission from: **a**,**b**, ref. 4, APS; **c**,**d**, ref. 9, Springer Nature Ltd; **e**, ref. 61 under a Creative Commons licence CC BY 4.0.

https://doi.org/10.1038/s41563-024-01962-5

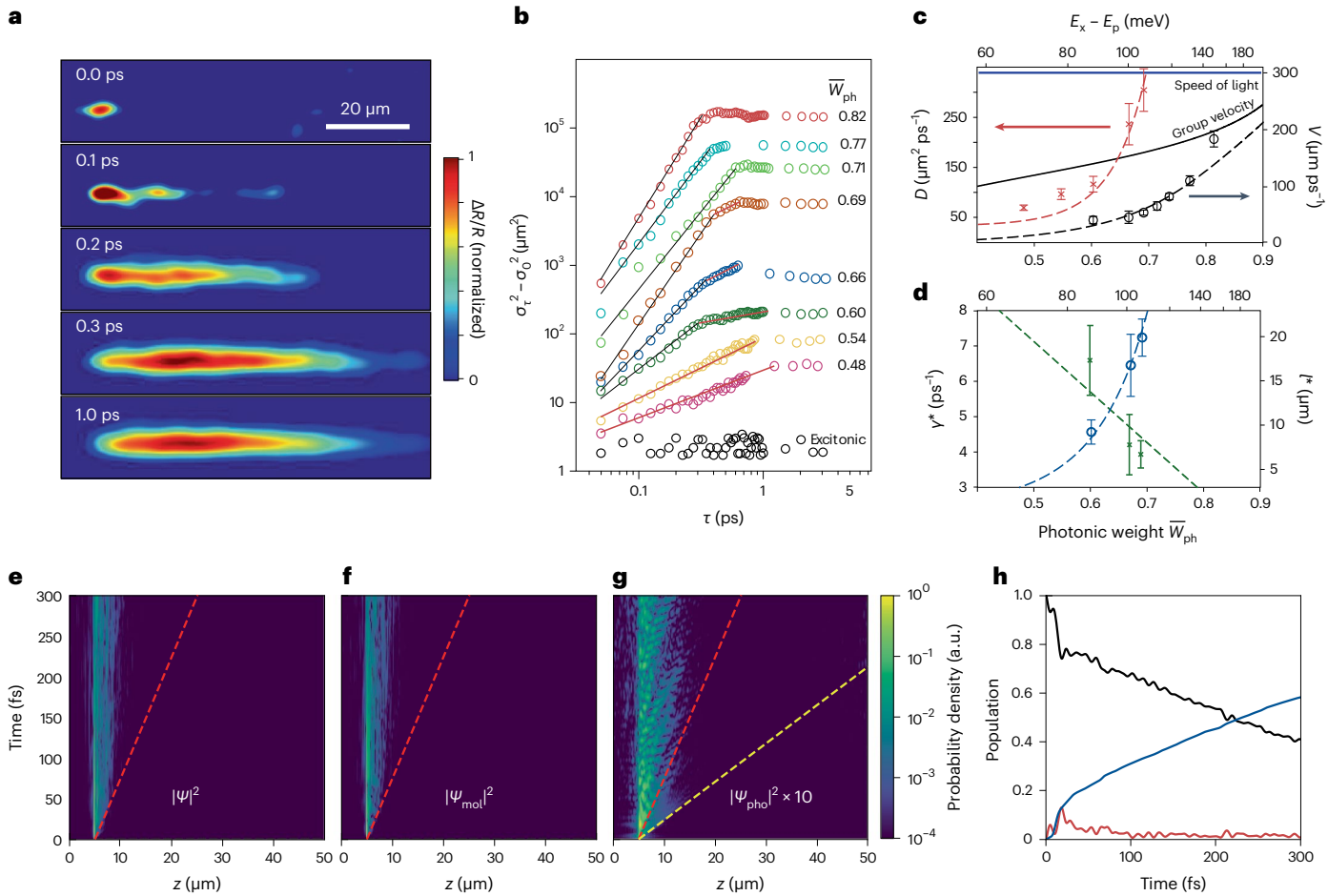

Fig. 4 | Ultrafast dynamics of cavity-enhanced transport. a, Snapshots of the spatial distribution of exciton–polaritons during ultralong-range propagation, acquired via femtosecond pump–probe microscopy. $\Delta R/R$, relative reflectivity change. **b**, Mean squared displacement (MSD; $\sigma_\tau^2 - \sigma_0^2$) as a function of time (τ), measured for polaritons with various photonic weight ($\overline{W}_{ph}$) values (note the double-logarithmic scale). The data can be fitted to a power-law expansion (MSD $\propto \tau^\beta$) with $\beta = 1$ (red solid lines) corresponding to diffusive expansion and $\beta = 2$ (black solid lines) corresponding to ballistic expansion. **c**, Diffusion coefficient (D; red crosses) and effective ballistic velocity (V; black open circles), as extracted from the propagation kinetics in **b**, as a function of the photonic weight (bottom axis) or the difference between the exciton (E_x) and polariton (E_p) energies (top axis). The solid black line marks the group velocity predicted by the polariton dispersion. The error bars represent the standard deviation obtained from repeated measurements at several locations on the sample. **d**, Polariton mean free path (l^*) and scattering rate (γ^*) as a function of the photonic weight. **e**–**g**, Simulation results, showing the spatio-temporal evolution of the polaritonic wavefunction $|\psi|^2$ (**e**), the molecular component $|\psi_{mol}|^2$ (**f**) and the photonic component $|\psi_{pho}|^2$ (**g**). The photonic component was multiplied by tenfold for visibility. The yellow and red dashed lines mark propagation at the maximum group velocities of the upper and lower polaritons, respectively. **h**, Photonic (red) and molecular (black) contributions to the total polaritonic wavefunction, and ground-state population (blue), as a function of time. Panels reproduced with permission from: **a**–**d**, ref. 21, Springer Nature Ltd; **e**–**h**, ref. 32 under a Creative Commons licence CC BY 4.0.

microscopy, long-range in-plane propagation over more than 100 μm was visualized directly (Fig. 3c). As seen in Fig. 3d, for polaritons whose energies were further away from that of the bare molecule (thus having larger photonic weights) the long-range propagation becomes more pronounced, as expected. Later, similar behaviour was also observed for molecules strongly coupled to SLR modes in plasmonic arrays[61,89]. Interestingly, in ref. 61 the propagation distance was observed to follow the inverse of Δk (Fig. 3e), the width of the dispersion curve along the in-plane wavenumber axis.

Whereas such steady-state experiments clearly confirmed the existence of long-range transport, its extent and its link with strong coupling, they could not provide direct information on the transport dynamics, the transport mechanism and a direct comparison with kinetic models. Early theoretical studies, which accounted for the molecular complexity, have shown that considering the polaritonic states as ideal, infinitely extended plane waves was an oversimplification[64–66,88,90] and therefore, deviations from a simple picture of a coherent wavepacket propagating freely through a dispersive medium (as, for example, light in an optical fibre) should be expected. To gain deeper insight into the transport dynamics, recent experimental studies began to apply ultrafast pump–probe microscopy techniques to strongly coupled organic cavities[10,19–23]. It was immediately observed that the polariton propagation was substantially slower than expected (considering the polariton group velocity), exhibiting signatures of non-ballistic transport[10,19]. In another study[20], it was also observed that the reduction in the polariton velocity followed the cavity loss rate, even though the polariton dispersion and the group velocity extracted from it are almost insensitive to the Q factor. This effect was attributed to the impact of the photon lifetime on the characteristics of the dark-state manifold and to population transfer between the polaritonic and the dark states[35,91].

Recently, a more comprehensive picture of long-range energy transport was obtained experimentally, by studying the spatio-temporal dynamics of BSW polaritons[21] and using energy/momentum-resolved pump–probe microscopy. The transport was found to have a ballistic nature—as is often assumed for polaritons—at

two-thirds the speed of light, and in agreement with the calculated group velocity. However, this purely ballistic motion was only attained for modes far detuned from the molecular exciton with relatively high photonic fractions of ~80%. At lower photonic fractions, a rich behaviour was uncovered by scanning across the lower polariton branch (Fig. 4). Specifically, these measurements showed a transition between ballistic transport over short distances and diffusive expansion at longer distances. The appearance of diffusion is generally attributed to multiple scattering, with the crossover from ballistic to diffusive transport occurring at a length scale set by the scattering mean free path. In addition, mesoscopic quantities that govern and characterize the transport, such as the mean free path, the diffusion coefficient and scattering rate, were extracted, including their variation with the polariton composition. The mean free path and scattering mean free time increase with the polariton photonic weight, which is in accordance with the general view that the scattering stems primarily from the molecular disorder (either static or dynamic)[66]. Importantly, even in the diffusive regime, diffusion coefficients of the order of 10^6 cm^2 s^{-1} were measured, representing an enhancement of more than seven orders of magnitude compared with typical excitonic materials, and clearly demonstrating the remarkable impact of strong coupling on the transport properties. Such dependence of the transport nature on the polariton composition was also observed for exciton–polaritons in layered halide perovskite microcavities[22]. Interestingly, this study also identified an initial acceleration stage under resonant excitation (before reaching a constant velocity), which was attributed to polariton–polariton interactions.

In parallel, QM/MM simulations, which accounted for the full molecular structure and the vibrational degrees of freedom[32] have successfully reproduced the observed transition between ballistic and diffusive transport. These simulations have also explained the central role of molecular vibrations in mediating the back-and-forth population transfer between the propagating polaritonic modes and the stationary dark states, which, in addition to reducing the effective velocity, renders the transport diffusive. This conclusion was supported by the experimental results of refs. 21,22, which also indicated that the transport dynamics are governed by thermally activated scattering. Therefore, apart from the direct dependence on the photonic weight, the propagation of each polaritonic subpopulation depends strongly on its energetic overlap with the bare-molecule absorption spectrum. On the other hand, it was also shown that the molecular disorder can give rise to localized polaritonic states[37], which indicates that, at finite temperatures, the (diffusive) transport is, to some extent, thermally assisted.

Conclusions and outlook

In summary, after more than a decade of intense research, it is already well established that strong coupling of molecules and photonic structures can enhance energy transport in organic semiconductors and intermolecular energy exchange by several orders of magnitude, in terms of both efficiency and the typical distances. This enhancement holds great promise for organic photovoltaics, organic light sources and other active optoelectronic devices, all of which can benefit from the superior energy flow endowed by strong coupling, along with the known advantages of organic materials (that is, facile processability, large material variety and chemical tunability, flexibility and so on). However, to fully harness the potential of cavity-enhanced transport, the inner workings of this phenomenon must first be deciphered. The past few years have witnessed several important first steps towards this goal, showing the important role of molecular disorder, thermal fluctuations and scattering, which cannot be ignored even under strong light–matter coupling. In addition, several experiments have already studied such enhanced transport effects in prototypical devices[48,92–94]. Nevertheless, many intriguing questions remain to be resolved in future research. For one, the microscopic scattering mechanisms of polaritons are not yet fully clear, and further investigation is required to understand to what extent the scattering is dominated by elastic versus inelastic (phase-destructive) effects. Such experiments will also shed light on the thermalization processes that lead to polariton condensation[40] and could be used to optimize and control polariton condensates and their dynamics. To this end, systematic temperature-dependent measurements will be extremely important, as well as extensive time-resolved spectroscopic studies that will probe the gradual loss of coherence in the system. Complementing experimental studies, theoretical modelling will play a key role in elucidating the microscopic mechanisms of polariton scattering, and in particular, the role of molecular vibrations in mediating the transport dynamics. For example, an unambiguous understanding of the processes of vibrationally assisted scattering (usually invoked in molecules with well-defined vibronic peaks in the absorption spectrum) and radiative pumping (which is more suitable for molecules with a broad absorption spectrum) and their relationship remains lacking, which is holding back the development of simple design rules for devices to make use of cavity-enhanced energy transfer and transport. It will be highly desirable to develop a theoretical framework that can capture enough of the complexity of the molecular structure, including the internal degrees of freedom, while being simple enough to enable its application in dispersive systems with macroscopic numbers of molecules. In addition, the accurate real-space modelling of optical platforms[95] is needed for quantitative predictions in specific device geometries.

In parallel to the research on cavity-enhanced energy transport, several experimental studies have obtained evidence of enhanced electrical conductivity under electronic strong coupling[96–98], pointing towards the possibility of cavity-enhanced charge transport. These promising results are supported by theoretical modelling[96,99], which has shown that cavity-induced long-range correlations in the charge-density oscillations may indeed give rise to such a phenomenon. However, with some conflicting results on this matter[100], the question of cavity-enhanced conductivity remains open and, as of today, it is still much less understood compared with cavity-enhanced energy transport. In that respect, time-resolved imaging techniques, in the spirit of refs. 10,20–22, could be developed to directly probe the spatio-temporal dynamics of charge carriers under strong coupling. Such experiments will elucidate the impact of strong coupling on conductance and will provide deeper insight into the mechanism of this fascinating and technologically important phenomenon.

In a broader context, the basic concepts underlying the enhanced transport are not limited to electronic excitations but apply equally to molecular vibrations and phonons. Indeed, several studies have started to look into transport phenomena under vibrational strong coupling[24,101–103]. Furthermore, in polar dielectric materials, hybrid excitations known as surface phonon polaritons can arise from the hybridization between EM surface waves and lattice vibrations[104]. With phonons being the carriers of thermal energy in insulating solids, their hybridization with the EM field can give rise to enhanced thermal conductivity in thin films[105,106], which has important implications for thermal management in electronics.

References

1. Garcia-Vidal, F. J., Ciuti, C. & Ebbesen, T. W. Manipulating matter by strong coupling to vacuum fields. *Science* **373**, eabd0336 (2021).
2. Li, T. E., Cui, B., Subotnik, J. E. & Nitzan, A. Molecular polaritonics: chemical dynamics under strong light–matter coupling. *Annu. Rev. Phys. Chem.* **73**, 43–71 (2022).
3. Birks, J. B. *Photophysics of Aromatic Molecules* (Wiley, 1970)
4. Aberra Guebrou, S. et al. Coherent emission from a disordered organic semiconductor induced by strong coupling with surface plasmons. *Phys. Rev. Lett.* **108**, 066401 (2012).

5. Shi, L. et al. Spatial coherence properties of organic molecules coupled to plasmonic surface lattice resonances in the weak and strong coupling regimes. *Phys. Rev. Lett.* **112**, 153002 (2014).
6. Feist, J. & Garcia-Vidal, F. J. Extraordinary exciton conductance induced by strong coupling. *Phys. Rev. Lett.* **114**, 196402 (2015).
7. Schachenmayer, J., Genes, C., Tignone, E. & Pupillo, G. Cavity-enhanced transport of excitons. *Phys. Rev. Lett.* **114**, 196403 (2015).
8. Gonzalez-Ballestero, C., Feist, J., Moreno, E. & Garcia-Vidal, F. J. Harvesting excitons through plasmonic strong coupling. *Phys. Rev. B* **92**, 121402 (2015).
9. Lerario, G. et al. High-speed flow of interacting organic polaritons. *Light Sci. Appl.* **6**, e16212 (2017).
10. Rozenman, G. G., Akulov, K., Golombek, A. & Schwartz, T. Long-range transport of organic exciton–polaritons revealed by ultrafast microscopy. *ACS Photon.* **5**, 105–110 (2018).
11. Coles, D. M. et al. Polariton-mediated energy transfer between organic dyes in a strongly coupled optical microcavity. *Nat. Mater.* **13**, 712–719 (2014).
12. Zhong, X. et al. Non-radiative energy transfer mediated by hybrid light–matter states. *Angew. Chem. Int. Ed.* **55**, 6202–6206 (2016).
13. Zhong, X. et al. Energy transfer between spatially separated entangled molecules. *Angew. Chem. Int. Ed.* **56**, 9034–9038 (2017).
14. Mikhnenko, O., Blom, P. & Nguyen, T. Exciton diffusion in organic semiconductors. *Energy Environ. Sci.* **8**, 1867–1888 (2015).
15. Cao, H. et al. Recent progress in degradation and stabilization of organic solar cells. *J. Power Sources* **264**, 168–183 (2014).
16. Sanvitto, D. & Kéna-Cohen, S. The road towards polaritonic devices. *Nat. Mater.* **15**, 1061–1073 (2016).
17. Wenus, J. et al. Hybrid organic–inorganic exciton–polaritons in a strongly coupled microcavity. *Phys. Rev. B.* **74**, 235212 (2006).
18. Paschos, G. G. et al. Hybrid organic–inorganic polariton laser. *Sci. Rep.* **7**, 11377 (2017).
19. Pandya, R. et al. Microcavity-like exciton–polaritons can be the primary photoexcitation in bare organic semiconductors. *Nat. Commun.* **12**, 6519 (2021).
20. Pandya, R. et al. Tuning the coherent propagation of organic exciton–polaritons through dark state delocalization. *Adv. Sci.* **9**, 2105569 (2022).
21. Balasubrahmaniyam, M. et al. From enhanced diffusion to ultrafast ballistic motion of hybrid light–matter excitations. *Nat. Mater.* **22**, 338–344 (2023).
22. Xu, D. et al. Ultrafast imaging of polariton propagation and interactions. *Nat. Commun.* **14**, 3881 (2023).
23. Jin, L. et al. Enhanced two-dimensional exciton propagation via strong light–matter coupling with surface lattice plasmons. *ACS Photon.* **10**, 1983–1991 (2023).
24. Xiang, B. et al. Intermolecular vibrational energy transfer enabled by microcavity strong light–matter coupling. *Science* **368**, 665–667 (2020).
25. DelPo, C. A. et al. Polariton decay in donor–acceptor cavity systems. *J. Phys. Chem. Lett.* **12**, 9774–9782 (2021).
26. Son, M. et al. Energy cascades in donor–acceptor exciton–polaritons observed by ultrafast two-dimensional white-light spectroscopy. *Nat. Commun.* **13**, 7305 (2022).
27. Sáez-Blázquez, R., Feist, J., Fernández-Domínguez, A. I. & García-Vidal, F. J. Organic polaritons enable local vibrations to drive long-range energy transfer. *Phys. Rev. B* **97**, 241407 (2018).
28. Reitz, M., Mineo, F. & Genes, C. Energy transfer and correlations in cavity-embedded donor–acceptor configurations. *Sci. Rep.* **8**, 9050 (2018).
29. Du, M. et al. Theory for polariton-assisted remote energy transfer. *Chem. Sci.* **9**, 6659–6669 (2018).
30. Schäfer, C., Ruggenthaler, M., Appel, H. & Rubio, A. Modification of excitation and charge transfer in cavity quantum-electrodynamical chemistry. *Proc. Natl Acad. Sci. USA* **116**, 4883–4892 (2019).
31. Chávez, N. C., Mattiotti, F., Méndez-Bermúdez, J. A., Borgonovi, F. & Celardo, G. L. Disorder-enhanced and disorder-independent transport with long-range hopping: application to molecular chains in optical cavities. *Phys. Rev. Lett.* **126**, 153201 (2021).
32. Sokolovskii, I., Tichauer, R. H., Morozov, D., Feist, J. & Groenhof, G. Multi-scale molecular dynamics simulations of enhanced energy transfer in organic molecules under strong coupling. *Nat. Commun.* **14**, 6613 (2023).
33. Engelhardt, G. & Cao, J. Unusual dynamical properties of disordered polaritons in microcavities. *Phys. Rev. B* **105**, 064205 (2022).
34. Wellnitz, D., Pupillo, G. & Schachenmayer, J. Disorder enhanced vibrational entanglement and dynamics in polaritonic chemistry. *Commun. Phys.* **5**, 120 (2022).
35. Tichauer, R. H., Sokolovskii, I. & Groenhof, G. Tuning the coherent propagation of organic exciton–polaritons through the cavity *Q*-factor. *Adv. Sci.* **10**, 2302650 (2023).
36. Aroeira, G. J. R., Kairys, K. T. & Ribeiro, R. F. Theoretical analysis of exciton wave packet dynamics in polaritonic wires. *J. Phys. Chem. Lett.* **14**, 5681–5691 (2023).
37. Engelhardt, G. & Cao, J. Polariton localization and dispersion properties of disordered quantum emitters in multimode microcavities. *Phys. Rev. Lett.* **130**, 213602 (2023).
38. Scholes, G. D. Long-range resonance energy transfer in molecular systems. *Annu. Rev. Phys. Chem.* **54**, 57–87 (2003).
39. Hakala, T. K. et al. Bose–Einstein condensation in a plasmonic lattice. *Nat. Phys.* **14**, 739–744 (2018).
40. Väkeväinen, A. I. et al. Sub-picosecond thermalization dynamics in condensation of strongly coupled lattice plasmons. *Nat. Commun.* **11**, 3139 (2020).
41. Freixanet, T., Sermage, B., Tiberj, A. & Thierry-Mieg, V. Propagation of excitonic polaritons in a microcavity. *Phys. Status Solidi A.* **178**, 133–138 (2000).
42. Myers, D. M. et al. Polariton-enhanced exciton transport. *Phys. Rev. B* **98**, 235302 (2018).
43. Liran, D., Rosenberg, I., West, K., Pfeiffer, L. & Rapaport, R. Fully guided electrically controlled exciton polaritons. *ACS Photon.* **5**, 4249–4252 (2018).
44. Hobson, P. A. et al. Strong exciton–photon coupling in a low-*Q* all-metal mirror microcavity. *Appl. Phys. Lett.* **81**, 3519–3521 (2002).
45. Miller, R. et al. Trapped atoms in cavity QED: coupling quantized light and matter. *J. Phys. B* **38**, S551 (2005).
46. Wang, S. et al. Quantum yield of polariton emission from hybrid light–matter states. *J. Phys. Chem. Lett.* **5**, 1433–1439 (2014).
47. Georgiou, K., Jayaprakash, R., Othonos, A. & Lidzey, D. G. Ultralong-range polariton-assisted energy transfer in organic microcavities. *Angew. Chem. Int. Ed.* **60**, 16661–16667 (2021).
48. Bhatt, P., Dutta, J., Kaur, K. & George, J. Long-range energy transfer in strongly coupled donor–acceptor phototransistors. *Nano Lett.* **23**, 5004–5011 (2023).
49. Maier, S. A. *Plasmonics: Fundamentals and Applications* (Springer, 2007)
50. Bellessa, J., Bonnand, C., Plenet, J. C. & Mugnier, J. Strong coupling between surface plasmons and excitons in an organic semiconductor. *Phys. Rev. Lett.* **93**, 036404 (2004).
51. Törmä, P. & Barnes, W. L. Strong coupling between surface plasmon polaritons and emitters: a review. *Rep. Prog. Phys.* **78**, 013901 (2015).

52. Pirotta, S. et al. Strong coupling between excitons in organic semiconductors and Bloch surface waves. *Appl. Phys. Lett.* **104**, 051111 (2014).
53. Lerario, G. et al. Room temperature Bloch surface wave polaritons. *Opt. Lett.* **39**, 2068–2071 (2014).
54. Abujetas, D. R., Feist, J., García-Vidal, F. J., Gómez Rivas, J. & Sánchez-Gil, J. A. Strong coupling between weakly guided semiconductor nanowire modes and an organic dye. *Phys. Rev. B* **99**, 205409 (2019).
55. Hao, Y.-W. et al. Hybrid-state dynamics of gold nanorods/dye J-aggregates under strong coupling. *Angew. Chem. Int. Ed.* **50**, 7824–7828 (2011).
56. Baranov, D. G., Wersäll, M., Cuadra, J., Antosiewicz, T. J. & Shegai, T. Novel nanostructures and materials for strong light–matter interactions. *ACS Photon.* **5**, 24–42 (2018).
57. Zengin, G. et al. Approaching the strong coupling limit in single plasmonic nanorods interacting with J-aggregates. *Sci. Rep.* **3**, 3074 (2013).
58. Chikkaraddy, R. et al. Single-molecule strong coupling at room temperature in plasmonic nanocavities. *Nature* **535**, 127–130 (2016).
59. Wang, W. et al. The rich photonic world of plasmonic nanoparticle arrays. *Mater. Today* **21**, 303–314 (2018).
60. Ramezani, M. et al. Dispersion anisotropy of plasmon–exciton–polaritons in lattices of metallic nanoparticles. *ACS Photon.* **5**, 233–239 (2018).
61. Berghuis, A. M. et al. Controlling exciton propagation in organic crystals through strong coupling to plasmonic nanoparticle arrays. *ACS Photon.* **9**, 2263–2272 (2022).
62. Castellanos, G. W., Bai, P. & Gómez Rivas, J. Lattice resonances in dielectric metasurfaces. *J. Appl. Phys.* **125**, 213105 (2019).
63. Tavis, M. & Cummings, F. W. Approximate solutions for an *N*-molecule-radiation-field Hamiltonian. *Phys. Rev.* **188**, 692–695 (1969).
64. Agranovich, V. M. & Gartstein, Y. N. Nature and dynamics of low-energy exciton polaritons in semiconductor microcavities. *Phys. Rev. B* **75**, 075302 (2007).
65. Michetti, P. & La Rocca, G. C. Polariton dynamics in disordered microcavities. *Physica E* **40**, 1926–1929 (2008).
66. Litinskaya, M. Propagation and localization of polaritons in disordered organic microcavities. *Phys. Lett. A* **372**, 3898–3903 (2008).
67. Manzano, D. A short introduction to the Lindblad master equation. *AIP Adv.* **10**, 025106 (2020).
68. Akselrod, G. M. et al. Visualization of exciton transport in ordered and disordered molecular solids. *Nat. Commun.* **5**, 3646 (2014).
69. Ishizaki, A. & Fleming, G. R. Unified treatment of quantum coherent and incoherent hopping dynamics in electronic energy transfer: reduced hierarchy equation approach. *J. Chem. Phys.* **130**, 234111 (2009).
70. Mirkovic, T. et al. Light absorption and energy transfer in the antenna complexes of photosynthetic organisms. *Chem. Rev.* **117**, 249–293 (2017).
71. del Pino, J., Schröder, F. A., Chin, A. W., Feist, J. & Garcia-Vidal, F. J. Tensor network simulation of non-Markovian dynamics in organic polaritons. *Phys. Rev. Lett.* **121**, 227401 (2018).
72. Groenhof, G. & Toppari, J. J. Coherent light harvesting through strong coupling to confined light. *J. Phys. Chem. Lett.* **9**, 4848–4851 (2018).
73. Fowler-Wright, P., Lovett, B. W. & Keeling, J. Efficient many-body non-Markovian dynamics of organic polaritons. *Phys. Rev. Lett.* **129**, 173001 (2022).
74. Pérez-Sánchez, J. B., Koner, A., Stern, N. P. & Yuen-Zhou, J. Simulating molecular polaritons in the collective regime using few-molecule models. *Proc. Natl Acad. Sci. USA* **120**, e2219223120 (2023).
75. Olaya-Castro, A. & Scholes, G. D. Energy transfer from Förster–Dexter theory to quantum coherent light-harvesting. *Int. Rev. Phys. Chem.* **30**, 49–77 (2011).
76. May, V. & Kühn, O. *Charge and Energy Transfer Dynamics in Molecular Systems* (Wiley, 2011)
77. Yang, M. & Fleming, G. R. Influence of phonons on exciton transfer dynamics: comparison of the Redfield, Förster, and modified Redfield equations. *Chem. Phys.* **275**, 355–372 (2002).
78. Gersten, J. I. & Nitzan, A. Accelerated energy transfer between molecules near a solid particle. *Chem. Phys. Lett.* **104**, 31–37 (1984).
79. Kobayashi, T., Zheng, Q. & Sekiguchi, T. Resonant dipole–dipole interaction in a cavity. *Phys. Rev. A* **52**, 2835–2846 (1995).
80. Agarwal, G. S. & Gupta, S. D. Microcavity-induced modification of the dipole–dipole interaction. *Phys. Rev. A* **57**, 667–670 (1998).
81. Kurizki, G. & Genack, A. Z. Suppression of molecular interactions in periodic dielectric structures. *Phys. Rev. Lett.* **61**, 2269–2271 (1988).
82. Hopmeier, M., Guss, W., Deussen, M., Göbel, E. O. & Mahrt, R. F. Enhanced dipole–dipole interaction in a polymer microcavity. *Phys. Rev. Lett.* **82**, 4118–4121 (1999).
83. Andrew, P. & Barnes, W. L. Energy transfer across a metal film mediated by surface plasmon polaritons. *Science* **306**, 1002–1005 (2004).
84. Bouchet, D., Cao, D., Carminati, R., De Wilde, Y. & Krachmalnicoff, V. Long-range plasmon-assisted energy transfer between fluorescent emitters. *Phys. Rev. Lett.* **116**, 037401 (2016).
85. Georgiou, K. et al. Control over energy transfer between fluorescent BODIPY dyes in a strongly coupled microcavity. *ACS Photon.* **5**, 258–266 (2018).
86. Garcia-Vidal, F. J. & Feist, J. Long-distance operator for energy transfer. *Science* **357**, 1357–1358 (2017).
87. Cargioli, A. et al. Active control of polariton-enabled long-range energy transfer. *Nanophotonics* **13**, 2541–2551 (2024).
88. Agranovich, V. M., Litinskaia, M. & Lidzey, D. G. Cavity polaritons in microcavities containing disordered organic semiconductors. *Phys. Rev. B* **67**, 085311 (2003).
89. Zakharko, Y. et al. Radiative pumping and propagation of plexcitons in diffractive plasmonic crystals. *Nano Lett.* **18**, 4927–4933 (2018).
90. Michetti, P. & La Rocca, G. C. Polariton states in disordered organic microcavities. *Phys. Rev. B* **71**, 115320 (2005).
91. Groenhof, G., Climent, C., Feist, J., Morozov, D. & Toppari, J. J. Tracking polariton relaxation with multiscale molecular dynamics simulations. *J. Phys. Chem. Lett.* **10**, 5476–5483 (2019).
92. Liu, B., Huang, X., Hou, S., Fan, D. & Forrest, S. R. Photocurrent generation following long-range propagation of organic exciton–polaritons. *Optica* **9**, 1029–1036 (2022).
93. Wang, M., Hertzog, M. & Börjesson, K. Polariton-assisted excitation energy channeling in organic heterojunctions. *Nat. Commun.* **12**, 1874 (2021).
94. Liu, B., Horowitz, J. & Forrest, S. R. Guided Bloch surface wave polaritons on patterned distributed Bragg reflectors at room temperature. *ACS Photon.* **10**, 4476–4482 (2023).
95. Zhou, Z., Chen, H.-T., Sukharev, M., Subotnik, J. E. & Nitzan, A. Nature of polariton transport in a Fabry–Pérot cavity. *Phys. Rev. A* **109**, 033717 (2024).
96. Orgiu, E. et al. Conductivity in organic semiconductors hybridized with the vacuum field. *Nat. Mater.* **14**, 1123–1129 (2015).
97. Nagarajan, K. et al. Conductivity and photoconductivity of a p-type organic semiconductor under ultrastrong coupling. *ACS Nano* **14**, 10219–10225 (2020).
98. Bhatt, P., Kaur, K. & George, J. Enhanced charge transport in two-dimensional materials through light–matter strong coupling. *ACS Nano* **15**, 13616–13622 (2021).

99. Hagenmüller, D., Schachenmayer, J., Schütz, S., Genes, C. & Pupillo, G. Cavity-enhanced transport of charge. *Phys. Rev. Lett.* **119**, 223601 (2017).
100. Kang, E. S. H. et al. Charge transport in phthalocyanine thin-film transistors coupled with Fabry–Pérot cavities. *J. Mater. Chem. C* **9**, 2368–2374 (2021).
101. Bylinkin, A. et al. Real-space observation of vibrational strong coupling between propagating phonon polaritons and organic molecules. *Nat. Photon.* **15**, 197–202 (2020).
102. Li, T. E., Nitzan, A. & Subotnik, J. E. Energy-efficient pathway for selectively exciting solute molecules to high vibrational states via solvent vibration–polariton pumping. *Nat. Commun.* **13**, 4203 (2022).
103. Suyabatmaz, E. & Ribeiro, R. F. Vibrational polariton transport in disordered media. *J. Chem. Phys.* **159**, 034701 (2023).
104. Agranovich, V. M. & Mills, D. L. (eds) *Surface Polaritons: Electromagnetic Waves at Surfaces and Interfaces* (North-Holland Publishing, 1982).
105. Chen, D.-Z. A., Narayanaswamy, A. & Chen, G. Surface phonon–polariton mediated thermal conductivity enhancement of amorphous thin films. *Phys. Rev. B* **72**, 155435 (2005).
106. Tranchant, L. et al. Two-dimensional phonon polariton heat transport. *Nano Lett.* **19**, 6924–6930 (2019).
107. Sáez Blázquez, R. *Dressing the Vacuum: Strong Light–Matter Coupling for Enhancing Photon Correlations and Exciton Transport*. PhD thesis, Universidad Autónoma de Madrid (2020).
108. Rider, M. S. & Barnes, W. L. Something from nothing: linking molecules with virtual light. *Contemp. Phys.* **62**, 217–232 (2022).
109. Roux, F. L., Taylor, R. A. & Bradley, D. D. C. Enhanced and polarization-dependent coupling for photoaligned liquid crystalline conjugated polymer microcavities. *ACS Photon.* **7**, 746–758 (2020).
110. Gonzalez-Ballestero, C., Feist, J., Gonzalo Badía, E., Moreno, E. & Garcia-Vidal, F. J. Uncoupled dark states can inherit polaritonic properties. *Phys. Rev. Lett.* **117**, 156402 (2016).
111. Botzung, T. et al. Dark state semilocalization of quantum emitters in a cavity. *Phys. Rev. B* **102**, 144202 (2020).

Author contributions
All authors contributed to the writing of this paper.

Competing interests
The authors declare no competing interests.

Additional information
Correspondence and requests for materials should be addressed to Johannes Feist, Francisco J. García-Vidal or Tal Schwartz.

Peer review information *Nature Materials* thanks Gregory Scholes and Joel Yuen-Zhou for their contribution to the peer review of this work.